

1 Exploring Predictive Performance: A Reanalysis of 2 the Geospace Model Transition Challenge

D. T. Welling,¹ B. J. Anderson,² G. Crowley,³ A. A. Pulkkinen,⁴ L.

Rastaetter,⁵

Corresponding author: D. T. Welling, Department of Climate and Space, University of Michigan, 2455 Hayward St., Ann Arbor, Michigan 48109, USA. (dwelling@umich.edu)

¹Department of Climate and Space,

This is the author manuscript accepted for publication and has undergone full peer review but has not been through the copyediting, typesetting, pagination and proofreading process, which may lead to differences between this version and the Version of Record. Please cite this article as doi:10.1002/2016SW001501

D R A F T February 14, 2017, 1:18pm

D R A F T

3 **Abstract.** The *Pulkkinen et al.* [2013] study evaluated the ability of five
4 different geospace models to predict surface dB/dt as a function of upstream
5 solar drivers. This was an important step in the assessment of research mod-
6 els for predicting and ultimately preventing the damaging effects of Geomag-
7 netically Induced Currents (GICs). Many questions remain concerning the
8 capabilities of these models. This study presents a reanalysis of the *Pulkki-*
9 *nen et al.* [2013] results in an attempt to better understand the models' per-

University of Michigan, Ann Arbor,
Michigan, USA.

²The Johns Hopkins University Applied
Physics Laboratory, Laurel, Maryland,
USA.

³Atmospheric and Space Technology
Research Associates, Boulder, Colorado,
USA

⁴Space Weather Laboratory, NASA
Goddard Space Flight Center, Greenbelt,
Maryland, USA

⁵Community Coordinated Modeling
Center, NASA Goddard Space Flight
Center, Greenbelt, Maryland, USA

10 formance. The range of validity of the models is determined by examining
11 the conditions corresponding to the empirical input data. It is found that
12 the empirical conductance models on which global magnetohydrodynamic
13 models rely are frequently used outside the limits of their input data. The
14 prediction error for the models is sorted as a function of solar driving and
15 geomagnetic activity. It is found that all models show a bias towards under-
16 prediction, especially during active times. These results have implications
17 for future research aimed at improving operational forecast models.

Author Manuscript

1. Introduction

18 Geomagnetically Induced Currents (GIC) remain an outstanding threat to technologi-
19 cal systems on which humans rely. The ultimate source of these currents are the in-
20 teraction between the solar wind and its embedded interplanetary magnetic field with
21 Earth's magnetosphere and ionosphere [Boteler, 2003]. This interaction drives variations
22 in the surface magnetic field, inducing GICs in the conducting lithosphere and any other
23 long conductor, including high-voltage power lines and oil pipelines. The effects of GICs
24 can damage these systems [Cannon *et al.*, 2013] and failures of the power grid, at great
25 economic loss, have been attributed to GICs [Davidson, 1940; Allen *et al.*, 1989; Boteler
26 *et al.*, 1998; Béland and Small, 2004]. Extreme space weather events could drive GICs
27 with widespread catastrophic consequences on the economy and society [Committee on
28 *the Societal and Economic Impacts of Severe Space Weather Events*, 2008].

29 A critical step to predicting and eventually mitigating the harmful effects of GICs is
30 predicting the ionospheric currents and variations of the surface magnetic field. Iono-
31 spheric and magnetospheric current densities can be combined with accurate knowledge
32 of Earth's impedance to calculate geoelectric field and estimate what portions of the power
33 grid are most at risk [Pirjola, 2002; Thomson *et al.*, 2009]. The time rate of change of the
34 surface magnetic field, dB/dt , is a direct indicator of geoelectric field strength [Viljanen
35 *et al.*, 2001]. To this end, it is important to develop, validate, and deploy forecast models
36 into an operational environment. This is one of the major themes of the recently released
37 National Space Weather Action Plan [National Science and Technology Council, 2015;
38 *Jonas and McCarron*, 2016].

39 An important first step towards the realization of operational GIC forecasting was
40 completed by *Pulkkinen et al.* [2013]. This study evaluated five models, both first-
41 principles-based and empirical, that predict surface dB/dt values from upstream solar
42 wind and interplanetary magnetic field (IMF) observations. Data-model comparisons
43 were made between six magnetometer observatories and corresponding model “virtual
44 magnetometers” across six space weather events spanning a range of activity. Binary
45 event analysis [*Jolliffe and Stephenson, 2003*] was used to evaluate each model’s ability
46 to forecast when surface dB/dt crossed different activity thresholds. The results of this
47 study were packaged into a report to NOAA’s Space Weather Prediction Center that
48 made recommendations concerning which models provided the most operational promise
49 (<http://ccmc.gsfc.nasa.gov/challenges/dBdt/>).

50 Despite the advances made by *Pulkkinen et al.* [2013], profound questions about the
51 performance and reliability of these five models persist. Each of these models, at some
52 level, relies on empirical relationships to perform part or all of the calculation. Over
53 what range of space weather conditions are these empirical relationships valid? When
54 do we leave these limits? Furthermore, the metrics used provide single-values to describe
55 performance across all events and activity levels. How does the model error vary with
56 geomagnetic conditions? Do the models perform equally as well during weak, strong, and
57 extreme driving?

58 This study attempts to answer these questions through reanalysis of the *Pulkkinen et al.*
59 [2013] results. The limits of the empirical inputs are identified for each model, and the
60 distribution of activity for these inputs is compared to the distribution of activity for the
61 six validation events. Data-model error is calculated and binned by solar and geomagnetic

62 activity to illustrate how each model performs as a function of strength of driving. This
63 analysis is repeated for cases where high and low latitude magnetometers are segregated.
64 These results are compared to illuminate patterns in model behavior and to investigate
65 how the error grows as input conditions exceed the limits of the models' empirical limits.

2. Review of Dataset & Models

66 To answer the above questions, the results from the *Pulkkinen et al.* [2013] study are
67 evaluated in greater depth. This study tested the ability of five models to predict surface
68 dB/dt over six separate space weather storm events. The events include the famous
69 Halloween Storm of October 29, 2003 [*Skoug et al.*, 2004; *Kappenman*, 2005]. Of the
70 five models tested, two are purely empirical and three are first-principles-based. All
71 data used in this study is freely available at NASA's Community Coordinated Modeling
72 Center (CCMC, <http://ccmc.gsfc.nasa.gov/challenges/dBdt>). Full details can be found
73 in *Pulkkinen et al.* [2013] and references therein.

74 The two empirical models include the Weimer Empirical Ground Magnetic Field Pre-
75 diction Model [*Weimer et al.*, 2010; *Weimer*, 2013] (herein referred to as "Weimer") and
76 the Weigel Empirical Ground Magnetic Field Prediction Model [*Weigel*, 2007; *Pulkkinen*
77 *et al.*, 2013] (herein referred to as "Weigel"). These models take separate approaches to
78 achieve the same goal: prediction of the perturbation of the surface magnetic field (ΔB)
79 as a function of upstream solar wind drivers. Note that ΔB is the perturbation of the field
80 from background levels, while dB/dt is the time derivative of ΔB . Each uses an extensive
81 input data set to build their empirical relationships, including hundreds of ground-based
82 magnetometer observations. The time range of input data for these models is listed in
83 the top two rows of Table 1.

84 The three remaining models are different implementations of global magnetohydrody-
 85 namic (MHD) models coupled to some ionospheric electrodynamic model. The generic
 86 formula for each is to use upstream solar wind observations to drive the model, then per-
 87 form Biot-Savart integrals of electric currents flowing through the magnetosphere, iono-
 88 sphere, and “gap-region” (the volume between the inner boundary of the MHD and the
 89 height of the ionosphere model) to predict ΔB [Yu *et al.*, 2010]. To obtain horizon-
 90 tal ionospheric currents, a Poisson-like equation is solved at a specified altitude using a
 91 prescribed conductance distribution. The conductance patterns are some combination
 92 of empirical and first-principles models whose inputs are F10.7 solar radio flux, MHD
 93 values about the inner boundary, and other parameterizations. The three models are
 94 Lyon-Fedder-Mobarry MHD model with the Magnetosphere-Ionosphere Coupler Solver
 95 (LFM-MIX, herein referred to as LFM [Wang *et al.*, 2004; Willberger *et al.*, 2004]), the
 96 Open General Geospace Circulation Model (OpenGGCM, [Raeder, 2003; Raeder *et al.*,
 97 2009]), and the Space Weather Modeling Framework (SWMF [Tóth *et al.*, 2005a; Tóth
 98 *et al.*, 2012]). While these models have been coupled to different inner magnetosphere
 99 models to improve ring current dynamics within the MHD results [De Zeeuw *et al.*, 2004;
 100 Pembroke *et al.*, 2012; Glocer *et al.*, 2013; Yu *et al.*, 2014], only the SWMF included this
 101 capability in the Pulkkinen *et al.* [2013] study.

The predictions of dB/dt from the five models were compared to observations from six
 ground-based magnetometers. For the purposes of Pulkkinen *et al.* [2013] and this study,
 dB/dt refers to the Pythagorean sum of the time derivatives of the two horizontal field
 components:

$$dB/dt \equiv (dB/dt)_H = \sqrt{(dB_x/dt)^2 + (dB_y/dt)^2} \quad (1)$$

102 where B_x and B_y are the north-south and east-west components, respectively, of the
103 surface field in geomagnetic dipole coordinates. Of the observatories used, three were
104 high-latitude stations ($> 65^\circ$ geomagnetic latitude) while three were mid-latitude ($> 50^\circ$).
105 Minute resolution data were used, yielding 56,880 data-model pairs per model across all six
106 events. Though the models are capable of producing higher time resolution output (MHD
107 models in particular have a history of investigating faster phenomena [*Claudepierre et al.*,
108 2009; *Hartinger et al.*, 2014, 2015]), 60 s sampling has been shown to capture most of the
109 variation; above these frequencies, the power spectrum falls off considerably [*Pulkkinen*
110 *et al.*, 2006].

3. Model Range of Validity

111 The first questions to be addressed are those pertaining to the range of validity of the
112 empirical models tested by *Pulkkinen et al.* [2013]. The range of validity is controlled by
113 model input data: if the model is run using solar wind drivers that do not fall within
114 the range of the solar wind drivers used to create the empirical relationship, there should
115 be no expectation that the model will return an accurate result. This is true because
116 the magnetosphere is a highly non-linear system [e.g., *Price and Prichard*, 1993; *Klimas*
117 *et al.*, 1996; *Shepherd*, 2007; *Borovsky*, 2014]; it is impossible to know *a priori* how
118 the magnetosphere will behave under increasingly strong driving. By comparing the
119 distribution of solar and geomagnetic activity covered by the six *Pulkkinen et al.* [2013]
120 events to the range of activity covered by empirical input data, judgments about the
121 appropriateness of each model can be made.

122 The top rows of Figures 1 and 2 illustrate the range of solar wind and geomag-
123 netic conditions covered by six events included in the *Pulkkinen et al.* [2013] study.

124 These plots show the distribution of minute-resolution solar wind electric field val-
125 ues (VB_Z , in mV/m , Figure 1) and Sym-H index values (nT , Figure 2) across all
126 six of the validation events. These data were obtained from the OMNI database
127 (http://omniweb.gsfc.nasa.gov/ow_min.html). The distributions are described using stan-
128 dard Tukey box plots [Frigge *et al.*, 1989]. The red lines show the median values, the boxes
129 contain 50% of all points and mark the first- and third- quartiles, and the whiskers mark
130 the last point within a distance of 1.5 times the interquartile range of the box. All other
131 points are considered outliers and are indicated by blue dots. The median VB_Z and Sym-
132 H values are $1.28 mV/m$ and $-44 nT$, respectively, indicating that the validation events
133 covered predominantly stormy periods. The maximum points of these distributions cor-
134 respond to the extreme conditions during the Halloween storm of 2003. The width of the
135 whisker diagrams demonstrate that a variety of conditions were covered by the six test
136 events.

137 The second and third box plots in Figures 1 and 2 show the distribution of VB_Z and
138 Sym-H values for times corresponding to input data for the Weimer and Weigel empirical
139 models (see Table 1). Because the input data time period for both of these models covers
140 the Halloween Storm (Oct. 29, 2003), the VB_Z maxima are the same as those for the
141 SWPC Event distribution (Figure 1, top box plot). The Weigel and Weimer models
142 include the subsequent extreme storms from November 2003, leading to minimum Sym-H
143 values that actually surpass those of the SWPC Sym-H distribution (Figure 2). Because
144 the maxima of the empirical model input data is not surpassed by any point included
145 in the test events, it is known that the *Pulkkinen et al.* [2013] validation study did not
146 exceed the range of validity for these models.

147 A deeper investigation of these distributions shows that while the data ranges are appro-
148 priate, the input data is strongly skewed towards weaker driving and activity compared to
149 the test event conditions. The VB_Z medians for Weimer and Weigel inputs are 0.03 and
150 0.01 mV/m , respectively, corresponding to almost no solar wind driving. The interquar-
151 tile ranges of these distributions are miniscule, demonstrating that 50% of all data points
152 used to construct the empirical relationships correspond to periods of negligible driving.
153 The situation is the same for the Sym-H distributions. Comparing to the distributions of
154 activity during the six test events, it becomes clear that the range of conditions tested by
155 the *Pulkkinen et al.* [2013] is not representative of the typical conditions used to create
156 these models. Based on input data alone, it may be expected that these models are more
157 likely to perform well during weak driving, where there is an abundance of input data.

158 A similar comparison for the three MHD models seems at first unintuitive because
159 these are first-principles, physics-based. However, there are is a key area where the MHD
160 models must turn to empirical relationships: ionospheric conductance. In addition to
161 contributions from solar extreme ultra violet photoionization, which is a slowly varying
162 and well-accounted-for source of conductance, each MHD code attempts to include con-
163 ductance sources from precipitating electrons. Both the LFM and OpenGGCM models
164 employ a chain of relationships to estimate precipitation from the MHD variables [*Raeder*,
165 2003; *Wiltberger et al.*, 2009]. These ultimately rely on the *Robinson et al.* [1987] empirical
166 formula to convert estimated electron precipitation to conductance. The SWMF uses a
167 different approach that ties conductance directly to field aligned current strength [*Ridley*
168 *et al.*, 2001]. This model was built via results from Assimilative Mapping of Ionospheric
169 Electrodynamics (AMIE, *Richmond and Kamide* [1988], which relies on a heavily modi-

170 fied empirical conductance model [*Spiro et al.*, 1982]). The AMIE results used to build
171 the SWMF empirical conductance model used only magnetometer data as input. Thus,
172 the ionospheric conductance models for each MHD code have a finite range of validity.
173 Conductance is an important value for MHD models [*Ridley et al.*, 2004; *Merkin et al.*,
174 2005a, b]. It affects both field-aligned and horizontal ionospheric currents, which strongly
175 drive surface ΔB and dB/dt values due to their proximity.

176 Judging from the range of input data, the empirical conductance models may be an
177 important limitation to the MHD models. The time span of input data for the *Robinson*
178 *et al.* [1987] relationship is limited to three moderate storm days [*Vickrey et al.*, 1981].
179 The relationship used in the SWMF was constructed using only a single month of AMIE
180 inputs [*Ridley et al.*, 2001]. The range of solar driving conditions and geomagnetic activity
181 during the time periods for which input data was used are illustrated in Figures 1 and 2,
182 respectively. Note that because the radar observations used to create the *Robinson et al.*
183 [1987] formula were taken in the late 1970s, predating standardized Sym-H, D_{ST} index
184 from the Kyoto World Data Center was used instead. While the median VB_Z values for
185 the MHD empirical conductance models (Figure 1, bottom two box plots) are similar to
186 the medians for the Weimer and Weigel models, the extreme values are far smaller: 2.52
187 and 2.30 mV/m , corresponding to weak driving. Similarly, the most extreme geomagnetic
188 conditions occurring during the input data time periods are -35 and -65 nT Sym-H/ D_{ST} .
189 These values represent weak to moderate driving and correspondingly moderate geomag-
190 netic activity. Clearly, the empirical models leveraged by these MHD models are being
191 exercised well beyond their range of validity.

4. Model Performance vs. Activity

Attention is now shifted to model performance as a function of solar and geomagnetic activity. For every data-model pair, a simple, normalized prediction error is calculated via,

$$Error = \frac{Y - X}{X} \quad (2)$$

where X is the observed value (either ΔB or dB/dt) and Y is the prediction. This normalization allows for the comparison between error during active periods (where perturbations are likely large) and calm periods (where perturbations are likely small). The error values are paired with the corresponding VB_Z and Sym-H values at the time the observation was made. The error is then binned by these values, yielding performance as a function of current space weather conditions. From these distributions, assessments can be made concerning the performance of the various models under different conditions and the connection, if any, to their empirical range of validity.

Figure 3 shows an example result from this analysis applied to the Weimer model. Each box plot represents the distribution of ΔB error values binned by VB_Z . Positive VB_Z values correspond to southward IMF; negative to northward IMF. The box plots are again Tukey box-and-whisker diagrams as in Figures 1 and 2; however, outliers are now excluded. The bin widths are 5 mV/m , ensuring most bins contain > 200 points. Because there are more southward than northward IMF periods covered in the *Pulkkinen et al.* [2013] study, several $VB_Z < 0$ bins contain fewer than 200 points, but all are above 30. A normalized error value of zero is a perfect prediction. Any values above zero are an overprediction: the model predicted a stronger ΔB value than observed. Inversely, any

209 values below zero are an underprediction, where the model predicted a lower ΔB value
210 than observed.

211 Figure 3 paints a picture of a model that predicts ΔB reasonably well. Most of the
212 medians (red lines) are slightly below zero, indicating there is a small bias towards un-
213 derprediction. Despite this bias, the distributions are well clustered about zero with most
214 interquartile ranges (which mark where 50% of the points lie) between $\pm 50\%$ error. Im-
215 portantly, the spread of the error (measured via the interquartile range and length of
216 the whiskers) is smaller and more regular during southward IMF conditions, when the
217 magnetosphere is most likely to be active. If ΔB error from the Weimer model is instead
218 binned versus Sym-H, the overall pattern does not change much (not shown).

219 Figure 4 repeats this analysis, but now examines dB/dt error and bins by Sym-H. The
220 bin width is now $25 nT$. The distribution of points per bin is more uniform; all bins
221 except the first two contain > 200 points. The comparison to Figure 3 is stark. The
222 medians are consistently well below zero, demonstrating an overwhelming bias towards
223 underprediction. The whiskers do not consistently cross above zero, showing that the
224 likelihood of an overprediction of dB/dt is quite low. This is especially true as Sym-
225 H becomes more negative, indicating stronger geomagnetic activity. A similar pattern
226 emerges if the error is binned by VB_Z (not shown).

227 Figure 5 shows that the Weimer model is in good company: all of the models included
228 in the *Pulkkinen et al. [2013]* study have a bias towards underpredicting dB/dt (bottom
229 two frames). The median error values, shown now as continuous line plots without the
230 box plot illustrations, are consistently below zero. This pattern emerges regardless of the
231 bin-type, either VB_Z (left hand frames) or Sym-H (right hand frames). For most models,

232 performance of ΔB prediction (top frames) is better (i.e., closer to zero). However, skill
233 in predicting the instantaneous magnetic perturbation does not appear to translate into
234 accurately capturing time dynamics.

235 Figure 6 illustrates how these results depend on latitude. The medians of the distri-
236 butions of normalized ΔB (left column) and dB/dt (right column) are shown when only
237 predictions for high-latitude magnetometers are included (dashed lines) and when only
238 predictions for mid-latitude magnetometers are included (dotted lines). For comparison,
239 the median values for all stations are shown as solid lines (same as in the top row of Figure
240 5). For the most part, there are not strong differences. However, during strong driving
241 ($VB_Z > 0$ mV/m) or strong geomagnetic activity (Sym-H < -200 nT), both the OpenG-
242 GCM (blue lines) and Weigel (green lines) models show a bias towards overprediction at
243 high latitude stations. Conversely, during the same regions, the SWMF model (orange
244 lines) overpredicts at mid-latitudes while underpredicting at higher locations.

245 Figure 7 shows a similar comparison, but for normalized dB/dt error. The differences
246 between latitudes are more muted than in Figure 6. Most of the latitude variation comes
247 from the three MHD models, with the two empirical models showing little distinguishing
248 features between high and mid-latitude error results.

5. Discussion

249 The inescapable conclusion of this study is that all of the models tested in the *Pulkkinen*
250 *et al.* [2013] have a strong predilection towards underprediction of surface dB/dt . This is
251 best illustrated in the lower right frame of Figure 5: the lines, representing median dB/dt
252 prediction error as a function of geomagnetic activity for each model, only cross zero at
253 three points. This means that an arbitrary prediction from any given model has more

254 than a 50% chance of yielding a dB/dt value that is lower than observed. As illustrated
255 in Figure 4, the odds can be much, much lower than 50%. Additional model development
256 will be required to produce models that can deliver low-error predictions in an operational
257 environment.

258 The results of this study reveal why the SWMF (orange lines in Figures 5, 6, and 7)
259 performed most favorably in the work of *Pulkkinen et al.* [2013]. The metrics leveraged
260 in *Pulkkinen et al.* [2013] tested whether a model's prediction crossed a given threshold.
261 Therefore, underpredictions are punished while overpredictions can still count as successful
262 predictions. Of the five models, the SWMF is least likely to underpredict dB/dt (Figure
263 5). This is especially true during strong solar driving ($VB_z > 10 \text{ mV/m}$) and during
264 periods of strong geomagnetic activity ($\text{Sym-H} < -150 \text{ nT}$). Such conditions were a focus
265 of the six test events. During periods of northward IMF (lower left-hand frame of Figure
266 5 where $VB_z < 0$), the SWMF stands as the only model that is very likely to overpredict
267 dB/dt . These characteristics are desirable when using a binary-event approach towards
268 validation.

269 An interesting consideration is the impact of the SWMF's inclusion of a ring current
270 model may be having on these results. Inclusion of such a model has been shown to
271 strengthen the ring current and region-2 Birkeland currents [*De Zeeuw et al.*, 2004; *Welling*
272 *et al.*, 2015]. It would be expected that these improvements would affect the mid-latitude
273 predictions most strongly, but still play a role in higher latitude results. Figure 6 appears
274 to support this as the SWMF is the least likely of any model to underpredict ΔB during
275 negative Sym-H conditions (right column). Figure 7 paints a more complicated picture
276 for dB/dt : while the SWMF performs better at high latitudes, the low latitude errors still

277 closer to zero than any other model. Further investigation is required, but these results
278 suggest that the improved ring current results are reducing prediction error.

279 This study also illustrates that skill in predicting field perturbation (ΔB) does not
280 directly translate accurate dB/dt . This is most evident with the two empirical models,
281 which perform reasonably well when predicting ΔB , yet severely underpredict the time
282 derivative. This was clearly illustrated for the Weimer model in Figures 3 and 4. The
283 empirical models excel at reproducing the field perturbation, but struggle to accurately
284 reproduce time dynamics. The MHD models, on the other hand, tend to be less likely
285 to underpredict dB/dt while showing no clear advantages in ΔB predictions. It may be
286 possible to compensate for this apparent disconnect by predicting dB/dt directly from
287 the magnitude, and not time derivative, of ΔB , as recently demonstrated by *Tóth et al.*
288 [2014]. It may be necessary to build the empirical models from dB/dt instead of ΔB .

289 Impulsive changes in the magnetosphere, such as storm sudden commencements, may
290 account for some of the dB/dt performance discrepancy between the MHD and empirical
291 models. SSCs can be clearly captured by the MHD codes. Indeed, during times of positive
292 Sym-H, which are typically the result of compressions of the magnetosphere from impulsive
293 changes in solar wind pressure, the MHD codes separate themselves from their empirical
294 brethren (Figure 5, lower-right frame). The Weimer model averages solar wind inputs over
295 20 minutes, likely reducing the impact of such impulses. The Weigel model includes an
296 impulsive component, but this was developed to capture dynamics on the order of hours
297 [*Weigel, 2007*]. Because the *Pulkkinen et al. [2013]* study focused on storms, dayside
298 compressions are common and are likely playing a role here.

299 Other captivating features manifest in these results without readily available explana-
300 tions. The SWMF, for example, tends to overpredict both ΔB and dB/dt under strongly
301 northward IMF conditions (i.e., negative VB_Z) in grandiose fashion. This feature stems
302 from the commencement and early main phases of the Halloween storm, where the SWMF
303 predicts strong perturbations associated with strongly northward IMF. There is no clear
304 reason why this pattern occurs. Additionally, there is a tendency for all models to un-
305 derpredict dB/dt during moderate conditions compared to quiet and extreme conditions.
306 Again, there is no obvious explanation for this behavior, and further research into the
307 models' behavior is required.

308 Candidate explanations for this behavior may be found by exploring limitations of this
309 study and that of *Pulkkinen et al.* [2013]. Uncertainty in the propagation of solar wind
310 drivers from L1 to the nose of the magnetosphere may be playing a role in the timing and
311 amplitude of dB/dt peaks. Studies have shown that the majority of propagation errors
312 are within ± 5 minutes [*Case and Wild*, 2012; *Hassan et al.*, 2015]. Reconnection rate in
313 ideal MHD models is always a point of concern. This is especially applicable in the tail,
314 where explosive reconnection is a requirement for capturing realistic substorm dynamics
315 which contribute strongly to nightside dB/dt . This is less of a concern on the dayside,
316 as MHD models have shown the ability to successfully mimic Petscheck reconnection
317 rates [*Ouellette et al.*, 2010, 2013] and reproduce the immediate ionospheric consequences
318 of dayside reconnection: cross polar cap potential (CPCP) dynamics and region 1 FAC
319 patterns [*Ridley et al.*, 2002; *Korth et al.*, 2008, 2011]. The MHD models have many
320 settings and parameters that affect the results [e.g., *Ridley et al.*, 2010], including grid
321 resolution. The MHD models leveraged by *Pulkkinen et al.* [2013] were configured to run

322 faster than real time using a modest computational allocation; it is unclear how the results
323 here would be affected if the models used different configurations or higher resolutions.
324 All of these limitations require further research to fully understand.

325 Finally, these results are placed back into the context of the range of validity. For the
326 two empirical models, there is little evidence that the input data bias towards weak driv-
327 ing and weak activity is impacting model performance. The Weimer and Weigel model
328 error does not grow significantly or systematically as a function of activity. The picture
329 grows even murkier when turning to the empirical conductance models embedded within
330 the MHD models. If the range of validity of the conductance models were indicated on
331 the various error plots, they would cover only a few of the VB_Z or Sym-H bins (inciden-
332 tally, it is noteworthy that the error medians of the three MHD models tend to converge
333 around the x-axis origins). Additionally, many assumptions and parameters feed into the
334 calculation of precipitation and conductance within MHD models. The full description of
335 the approach leveraged by the LFM model includes four different parameters chosen to
336 optimize a limited number of simulations [Wiltberger *et al.*, 2009]. This makes drawing
337 concrete conclusions about the Robinson *et al.* [1987] model very difficult as it is only
338 one step in the entire process. Despite these confounding factors, expanding the range
339 of validity for the conductance models by including data from geomagnetically active pe-
340 riods will almost certainly have a positive effect on the error patterns. Indeed, studies
341 that change only the conductance model show strong differences in cross polar cap poten-
342 tials [Merkin *et al.*, 2007]. Updating conductance models should be considered a priority
343 by the community. Alternatively, MHD coupling to advanced, physics-based ionosphere-
344 thermosphere models (a capability that exists in different forms [Raeder, 2003; Ridley

345 *et al.*, 2003; *Tóth et al.*, 2005b; *Merkin and Lyon*, 2010]), should be developed, leveraged,
346 and validated.

6. Conclusions

347 This study performed a reanalysis of the *Pulkkinen et al.* [2013] validation effort. It
348 determined the range of validity for the five models evaluated and compared them to the
349 range of activity used to exercise the codes. Model error for ΔB and dB/dt was binned by
350 solar driving (VB_Z) and geomagnetic activity (Sym-H) to explore how this error changes
351 as a function of those values. This analysis was repeated for high- and mid-latitude
352 magnetometers in isolation. From this analysis, the following conclusions were made:

- 353 • Because their input data is drawn primarily from periods of weak activity, the con-
354 ductance models upon which the MHD codes rely are frequently being used outside their
355 range of validity.
- 356 • All models included in the *Pulkkinen et al.* [2013] show a bias towards underprediction
357 of dB/dt . This behavior appears unrelated to performance of ΔB prediction.
- 358 • The SWMF is the least likely to underpredict dB/dt , which explains this model's
359 superior performance in the *Pulkkinen et al.* [2013] study. The inclusion of a ring current
360 model appears to be a contributing factor.

361 These results have implications for future research aimed at improving operational fore-
362 cast models. The range of validity analysis paints the MHD empirical conductance models
363 as liabilities. Investigating the impact of improvements or replacements will provide great
364 insight into MHD capabilities. Similarly, a deeper study of MHD coupling to ring current
365 models will reveal how important this feature is to both high and mid-latitude predictions.

366 Determining the relationship between the more accurate ΔB predictions and dB/dt , espe-
367 cially concerning the empirical models, may yield fast improvements to dB/dt predictions.
368 Preliminary work in this direction has shown promise [Tóth *et al.*, 2014]. Finally, it is
369 important to remember that these results are based on six event studies. Validation is
370 an ongoing process and expanding the number of data-model comparisons is critical for a
371 complete understanding of performance and limitations.

372 **Acknowledgments.** This project is a result of the efforts of the Geomagnet-
373 ically Induced Currents Working Group, a NASA Living With a Star Institute.
374 Solar wind and geomagnetic index data was provided by the OMNI database at
375 <http://omniweb.gsfc.nasa.gov>. Model and observations used in this and previous stud-
376 ies can be obtained from the NASA Community Coordinated Modeling Center at
377 <http://ccmc.gsfc.nasa.gov/challenges/dBdt>. The results presented in this paper rely on
378 the data collected at various geomagnetic observatories. We thank these institutions
379 for supporting its operation and INTERMAGNET for promoting high standards of mag-
380 netic observatory practice (www.intermagnet.org). D_{ST} index was obtained via the Kyoto
381 World Data Center (<http://wdc.kugi.kyoto-u.ac.jp>)

References

- 382 Allen, J., H. Sauer, L. Frank, and P. Reiff (1989), Effects of the March 1989 solar activity,
383 *Eos, Transactions American Geophysical Union*, 70(46), 1479, doi:10.1029/89EO00409.
384 Béland, J., and K. Small (2004), Space Weather Effects on Power Transmission Sys-
385 tems: The Cases of Hydro-Québec and Transpower New ZealandLtd, in *Effects of Space*
386 *Weather on Technology Infrastructure*, pp. 287–299, Kluwer Academic Publishers, Dor-

- 387 recht.
- 388 Borovsky, J. E. (2014), Canonical correlation analysis of the combined solar wind and
389 geomagnetic index data sets, *Journal of Geophysical Research: Space Physics*, 119(7),
390 5364–5381, doi:10.1002/2013JA019607.
- 391 Boteler, D. H. (2003), Geomagnetic Hazards to Conducting Networks, *Natural Hazards*,
392 28(2/3), 537–561, doi:10.1023/A:1022902713136.
- 393 Boteler, D. H., R. J. Pirjola, and H. Nevanlinna (1998), The effects of geomagnetic distur-
394 bances on electrical systems at the Earth’s surface, *Advances in Space Research*, 22(1),
395 17–27, doi:10.1016/S0273-1177(97)01096-X.
- 396 Cannon, P., et al. (2013), Extreme space weather: impacts on engineered systems and
397 infrastructure.
- 398 Case, N. A., and J. A. Wild (2012), A statistical comparison of solar wind propagation
399 delays derived from multispacecraft techniques, *Journal of Geophysical Research: Space*
400 *Physics*, 117(A2), doi:10.1029/2011JA016946.
- 401 Claudepierre, S. G., M. Wiltberger, S. R. Elkington, W. Lotko, and M. K. Hudson (2009),
402 Magnetospheric cavity modes driven by solar wind dynamic pressure fluctuations, *Geo-*
403 *physical Research Letters*, 36(13), L13,101, doi:10.1029/2009GL039045.
- 404 Committee on the Societal and Economic Impacts of Severe Space Weather Events (2008),
405 Workshop Report, *Tech. rep.*, Washington, D.C., doi:10.17226/12507.
- 406 Davidson, W. F. (1940), No TitleThe magnetic storm of March 24, 1940Effects in the
407 power system, *Edison Electric Institute Bulletin*.
- 408 De Zeeuw, D., S. Sazykin, R. Wolf, T. Gombosi, A. Ridley, and G. Tóth (2004), Coupling
409 of a global MHD code and an inner magnetosphere model: Initial results, *J. Geophys.*

- 410 *Res.*, 109(A12), A12,219, doi:10.1029/2003JA010,366.
- 411 Frigge, M., D. C. Hoaglin, and B. Iglewicz (1989), Some Implementations of the Boxplot,
412 *The American Statistician*, 43(1), 50, doi:10.2307/2685173.
- 413 Glocer, A., M. Fok, X. Meng, G. Toth, N. Buzulukova, S. Chen, and K. Lin (2013), CRCM
414 + BATS-R-US two-way coupling, *Journal of Geophysical Research: Space Physics*,
415 118(4), 1635–1650, doi:10.1002/jgra.50221.
- 416 Hartinger, M. D., D. T. Welling, N. M. Viall, M. B. Moldwin, and A. Ridley (2014),
417 The effect of magnetopause motion on fast mode resonance, *Journal of Geophysical*
418 *Research: Space Physics*, 119(10), 8212–8227, doi:10.1002/2014JA020401.
- 419 Hartinger, M. D., F. Plaschke, M. O. Archer, D. T. Welling, M. B. Moldwin, and A. Ridley
420 (2015), The global structure and time evolution of dayside magnetopause surface eigen-
421 modes, *Geophysical Research Letters*, 42(8), 2594–2602, doi:10.1002/2015GL063623.
- 422 Hassan, E., S. K. Morley, and J. T. Steinberg (2015), A statistical ensemble for solar wind
423 measurements: A step toward forecasting, in *2015 Los Alamos Space Weather Summer*
424 *School Research Reports*, edited by M. M. Cowee, pp. 17–31, Los Alamos National
425 Laboratory, Los Alamos.
- 426 Jolliffe, I., and D. Stephenson (2003), *Forecast Verification: A Practitioner's Guide in*
427 *Atmospheric Science*, Wiley, Hoboken, New Jersey.
- 428 Jonas, S., and E. D. McCarron (2016), White House Releases National Space Weather
429 Strategy and Action Plan, *Space Weather*, 14(2), 54–55, doi:10.1002/2015SW001357.
- 430 Kappenman, J. G. (2005), An overview of the impulsive geomagnetic field disturbances
431 and power grid impacts associated with the violent Sun-Earth connection events of 29-
432 31 October 2003 and a comparative evaluation with other contemporary storms, *Space*

- 433 *Weather*, 3(8), doi:10.1029/2004SW000128.
- 434 Klimas, A. J., D. Vassiliadis, D. N. Baker, and D. A. Roberts (1996), The organized non-
435 linear dynamics of the magnetosphere, *Journal of Geophysical Research: Space Physics*,
436 101(A6), 13,089–13,113, doi:10.1029/96JA00563.
- 437 Korth, H., B. J. Anderson, J. G. Lyon, and M. Wiltberger (2008), Comparison of Birkeland
438 current observations during two magnetic cloud events with MHD simulations, *Annales*
439 *Geophysicae*, 26(3), 499–516, doi:10.5194/angeo-26-499-2008.
- 440 Korth, H., L. Rastätter, B. J. Anderson, and a. J. Ridley (2011), Comparison of the
441 observed dependence of large-scale Birkeland currents on solar wind parameters with
442 that obtained from global simulations, *Annales Geophysicae*, 29(10), 1809–1826, doi:
443 10.5194/angeo-29-1809-2011.
- 444 Merkin, V., A. Sharma, K. Papadopoulos, G. Milikh, J. Lyon, and C. Goodrich (2005a),
445 Relationship between the ionospheric conductance, field aligned current, and magne-
446 topause geometry: Global MHD simulations, *Planetary and Space Science*, 53(9), 873–
447 879, doi:10.1016/j.pss.2005.04.001.
- 448 Merkin, V. G., and J. G. Lyon (2010), Effects of the low-latitude ionospheric boundary
449 condition on the global magnetosphere, *Journal of Geophysical Research: Space Physics*,
450 115(A10), doi:10.1029/2010JA015461.
- 451 Merkin, V. G., G. Milikh, K. Papadopoulos, J. Lyon, Y. S. Dimant, A. S. Sharma,
452 C. Goodrich, and M. Wiltberger (2005b), Effect of anomalous electron heating on the
453 transpolar potential in the LFM global MHD model, *Geophysical Research Letters*,
454 32(22), doi:10.1029/2005GL023315.

- 455 Merkin, V. G., M. J. Owens, H. E. Spence, W. J. Hughes, and J. M. Quinn (2007),
456 Predicting magnetospheric dynamics with a coupled Sun-to-Earth model: Challenges
457 and first results, *Space Weather*, 5(12), doi:10.1029/2007SW000335.
- 458 National Science and Technology Council (2015), National Space Weather Action Plan,
459 *Tech. rep.*
- 460 Ouellette, J. E., B. N. Rogers, M. Wiltberger, and J. G. Lyon (2010), Magnetic recon-
461 nection at the dayside magnetopause in global Lyon-Fedder-Mobarry simulations, *Journal*
462 *of Geophysical Research*, 115(A8), A08,222, doi:10.1029/2009JA014886.
- 463 Ouellette, J. E., O. J. Brambles, J. G. Lyon, W. Lotko, and B. N. Rogers (2013), Properties
464 of outflow-driven sawtooth substorms, *Journal of Geophysical Research: Space Physics*,
465 118(6), 3223–3232, doi:10.1002/jgra.50309.
- 466 Pembroke, A., F. Toffoletto, S. Sazykin, M. Wiltberger, J. Lyon, V. Merkin, and
467 P. Schmitt (2012), Initial results from a dynamic coupled magnetosphere-ionosphere-
468 ring current model, *Journal of Geophysical Research*, 117(A2), A02,211, doi:
469 10.1029/2011JA016979.
- 470 Pirjola, R. (2002), Review On The Calculation Of Surface Electric And Magnetic Fields
471 And Of Geomagnetically Induced Currents In Ground-Based Technological Systems,
472 *Surveys in Geophysics*, 23(1), 71–90, doi:10.1023/A:1014816009303.
- 473 Price, C. P., and D. Prichard (1993), The non-linear response of the magnetosphere: 30
474 October 1978, *Geophysical Research Letters*, 20(9), 771–774, doi:10.1029/93GL00844.
- 475 Pulkkinen, A., A. Viljanen, and R. Pirjola (2006), Estimation of geomagneti-
476 cally induced current levels from different input data, *Space Weather*, 4(8), doi:
477 10.1029/2006SW000229.

- 478 Pulkkinen, A., et al. (2013), Community-wide validation of geospace model ground mag-
479 netic field perturbation predictions to support model transition to operations, *Space*
480 *Weather*, *11*(6), 369–385, doi:10.1002/swe.20056.
- 481 Raeder, J. (2003), Global Magnetohydrodynamics - A Tutorial, in *Space Plasma Simula-*
482 *tion, Lecture Notes in Physics, Berlin Springer Verlag*, vol. 615, edited by J. Büchner,
483 C. Dum, and M. Scholer, p. 212.
- 484 Raeder, J., D. Larson, W. Li, E. L. Kepko, and T. Fuller-Rowell (2009), OpenGGCM
485 Simulations for the THEMIS Mission, in *The THEMIS Mission*, pp. 535–555, Springer
486 New York, New York, NY.
- 487 Richmond, A., and Y. Kamide (1988), Mapping electrodynamic features of the high-
488 latitude ionosphere from localized observations: Technique, *J. Geophys. Res.*, *93*, 5741–
489 5759.
- 490 Ridley, A., D. L. De Zeeuw, T. I. Gombosi, and K. G. Powell (2001), Using steady-state
491 MHD results to predict the global state of the magnetosphere-ionosphere system, *J.*
492 *Geophys. Res.*, *106*, 30,067–30,076.
- 493 Ridley, A., T. Gombosi, D. L. De Zeeuw, C. Clauer, and A. Richmond (2003), Ionospheric
494 control of the magnetospheric configuration: Neutral winds, *J. Geophys. Res.*, *108*,
495 2002JA009,464.
- 496 Ridley, A., T. Gombosi, and D. L. De Zeeuw (2004), Ionospheric control of the magneto-
497 spheric configuration: Conductance, *Ann. Geophys.*, *22*, 567–584.
- 498 Ridley, A. J., K. C. Hansen, G. Tóth, D. L. De Zueew, T. I. Gombosi, and K. G. Pow-
499 ell (2002), University of Michigan MHD results of the GGCM metrics challenge, *J.*
500 *Geophys. Res.*, *107*(A10), 1290, doi:10.1029/2001JA000,253.

- 501 Ridley, A. J., T. I. Gombosi, I. V. Sokolov, G. Tóth, and D. T. Welling (2010), Numerical
502 considerations in simulating the global magnetosphere, *Annales Geophysicae*, *28*(8),
503 1589–1614, doi:10.5194/angeo-28-1589-2010.
- 504 Robinson, R., R. Vondrak, K. Miller, T. Dabbs, and D. Hardy (1987), On calculating iono-
505 spheric conductances from the flux and energy of precipitating electrons, *J. Geophys.*
506 *Res.*, *92*, 2565.
- 507 Shepherd, S. G. (2007), Polar cap potential saturation: Observations, theory, and mod-
508 eling, *Journal of Atmospheric and Solar-Terrestrial Physics*, *69*(3), 234–248, doi:
509 10.1016/j.jastp.2006.07.022.
- 510 Skoug, R. M., J. T. Gosling, J. T. Steinberg, D. J. McComas, C. W. Smith, N. F. Ness,
511 Q. Hu, and L. F. Burlaga (2004), Extremely high speed solar wind: 2930 October 2003,
512 *Journal of Geophysical Research*, *109*(A9), A09,102, doi:10.1029/2004JA010494.
- 513 Spiro, R. W., P. H. Reiff, and L. J. Maher (1982), Precipitating electron energy flux
514 and auroral zone conductances-An empirical model, *Journal of Geophysical Research*,
515 *87*(A10), 8215, doi:10.1029/JA087iA10p08215.
- 516 Thomson, A., A. McKay, and A. Viljanen (2009), A review of progress in modelling of
517 induced geoelectric and geomagnetic fields with special regard to induced currents, *Acta*
518 *Geophysica*, *57*(1), 209–219.
- 519 Tóth, G., et al. (2005a), Space weather modeling framework: A new tool for the space
520 science community, *J. Geophys. Res.*, *110*, doi:doi:10.1029/2005JA011126.
- 521 Tóth, G., et al. (2005b), Space weather modeling framework: A new tool for the space
522 science community, *J. Geophys. Res.*, *110*, A12,226, doi:10.1029/2005JA011126.

- 523 Tóth, G., et al. (2012), Adaptive numerical algorithms in space weather modeling, *Journal*
524 *of Computational Physics*, *231*(3), 870–903, doi:10.1016/j.jcp.2011.02.006.
- 525 Tóth, G., X. Meng, T. I. Gombosi, and L. Rastätter (2014), Predicting the time deriva-
526 tive of local magnetic perturbations, *Journal of Geophysical Research: Space Physics*,
527 *119*(1), 310–321, doi:10.1002/2013JA019456.
- 528 Vickrey, J., R. Vondrak, and S. Matthews (1981), The diurnal and latitudinal variation
529 of auroral zone ionospheric conductivity, *J. Geophys. Res.*, *86*, 67.
- 530 Viljanen, A., H. Nevanlinna, K. Pajunpää, and A. Pulkkinen (2001), Time derivative of
531 the horizontal geomagnetic field as an activity indicator, *Annales Geophysicae*, *19*(9),
532 1107–1118.
- 533 Wang, W., M. Wiltberger, A. Burns, S. Solomon, T. Killeen, N. Maruyama, and J. Lyon
534 (2004), Initial results from the coupled magnetosphere – ionosphere – thermosphere
535 model: thermosphere – ionospheric responses, *J. Atmos. Sol-Terr. Phys.*, *66*, 1425.
- 536 Weigel, R. S. (2007), Solar wind time history contribution to the day-of-year variation
537 in geomagnetic activity, *Journal of Geophysical Research: Space Physics*, *112*(A10),
538 doi:10.1029/2007JA012324.
- 539 Weimer, D. R. (2013), An empirical model of ground-level geomagnetic perturbations,
540 *Space Weather*, *11*(3), 107–120, doi:10.1002/swe.20030.
- 541 Weimer, D. R., C. R. Clauer, M. J. Engebretson, T. L. Hansen, H. Gleisner, I. Mann,
542 and K. Yumoto (2010), Statistical maps of geomagnetic perturbations as a function
543 of the interplanetary magnetic field, *Journal of Geophysical Research: Space Physics*,
544 *115*(A10), doi:10.1029/2010JA015540.

- 545 Welling, D. T., V. K. Jordanova, A. Glocer, G. Toth, M. W. Liemohn, and D. R.
546 Weimer (2015), The two-way relationship between ionospheric outflow and the ring
547 current, *Journal of Geophysical Research: Space Physics*, *120*(6), 4338–4353, doi:
548 10.1002/2015JA021231.
- 549 Wiltberger, M., W. Wang, A. Burns, S. Solomon, J. Lyon, and C. Goodrich (2004),
550 Initial results from the coupled magnetosphere ionosphere thermosphere model: mag-
551 netospheric and ionospheric response, *J. Atmos. Sol-Terr. Phys.*, *66*, 1411.
- 552 Wiltberger, M., R. S. Weigel, W. Lotko, and J. a. Fedder (2009), Modeling seasonal varia-
553 tions of auroral particle precipitation in a global-scale magnetosphere-ionosphere simu-
554 lation, *Journal of Geophysical Research*, *114*(A1), A01,204, doi:10.1029/2008JA013108.
- 555 Yu, Y., A. J. Ridley, D. T. Welling, and G. Tóth (2010), Including gap region field-aligned
556 currents and magnetospheric currents in the MHD calculation of ground-based mag-
557 netic field perturbations, *Journal of Geophysical Research (Space Physics)*, *115*(A14),
558 A08,207, doi:10.1029/2009JA014869.
- 559 Yu, Y., V. Jordanova, D. T. Welling, B. Larsen, S. G. Claudepierre, and C. Kletzing
560 (2014), The role of ring current particle injections: Global simulations and Van Allen
561 Probes observations during 17 March 2013 storm, *Geophysical Research Letters*, *41*(4),
562 1126–1132, doi:10.1002/2014GL059322.

Model Name	Input Observations	Date Range
Weigel	Ground-based magnetometers	Jan. 2000 - Dec. 2006 (7 years)
Weimer	Ground-based magnetometers	Feb. 1998 - Dec. 2005 (8 years)
SWMF	AMIE-Ridley	Jan. 1997 (1 month)
LFM & OpenGGCM	Chatanika radar	Nov. 13, 17 1976 & April 6, 1977 (3 days)

Table 1. Time coverage (right most column) of input data (center column) for the various empirical models (leftmost column) ranges from comprehensive (Weigel and Weimer models, top two rows) to very sparse (SWMF, LFM, and OpenGGCM models, bottom two rows).

Figure 1. Distributions of solar wind electric field (VB_Z , mV/m) for every minute during the six validation events (top box plot, labeled “SWPC”) and for every minute corresponding to empirical input data for the Weimer & Weigel models (2nd and 3rd box plots) and for the empirical conductance models used by the MHD models (bottom two box plots). Box plots show median values (red lines), first- and third-quartiles (boxes), and range of data excluding outliers (whiskers). Outliers, defined as any point outside of the box by a distance of 1.5 times the interquartile range, are shown as dots. Positive VB_Z values indicate times of southward IMF, negative values indicate northward IMF. Minimum, maximum, and median values are listed in grey.

Figure 2. Same as Figure 1 but for Sym-H index values. Data is arranged such that more negative values, which indicate periods of stronger geomagnetic activity, are to the right. For time periods that predate the standard Sym-H index, Kyoto D_{ST} is used instead.

Figure 3. Normalized ΔB error distributions (y-axis and box plots) as a function of solar wind electric field (x-axis, mV/m) for the Weimer model. Box plot interpretation follows that of Figures 1 and 2. Positive error values represent overpredictions, negative values represent underpredictions.

Figure 4. Similar to Figure 3 but for normalized dB/dt error as a function of Sym-H. The x-axis is arranged so that negative Sym-H values, which correspond to higher geomagnetic activity, are to the right.

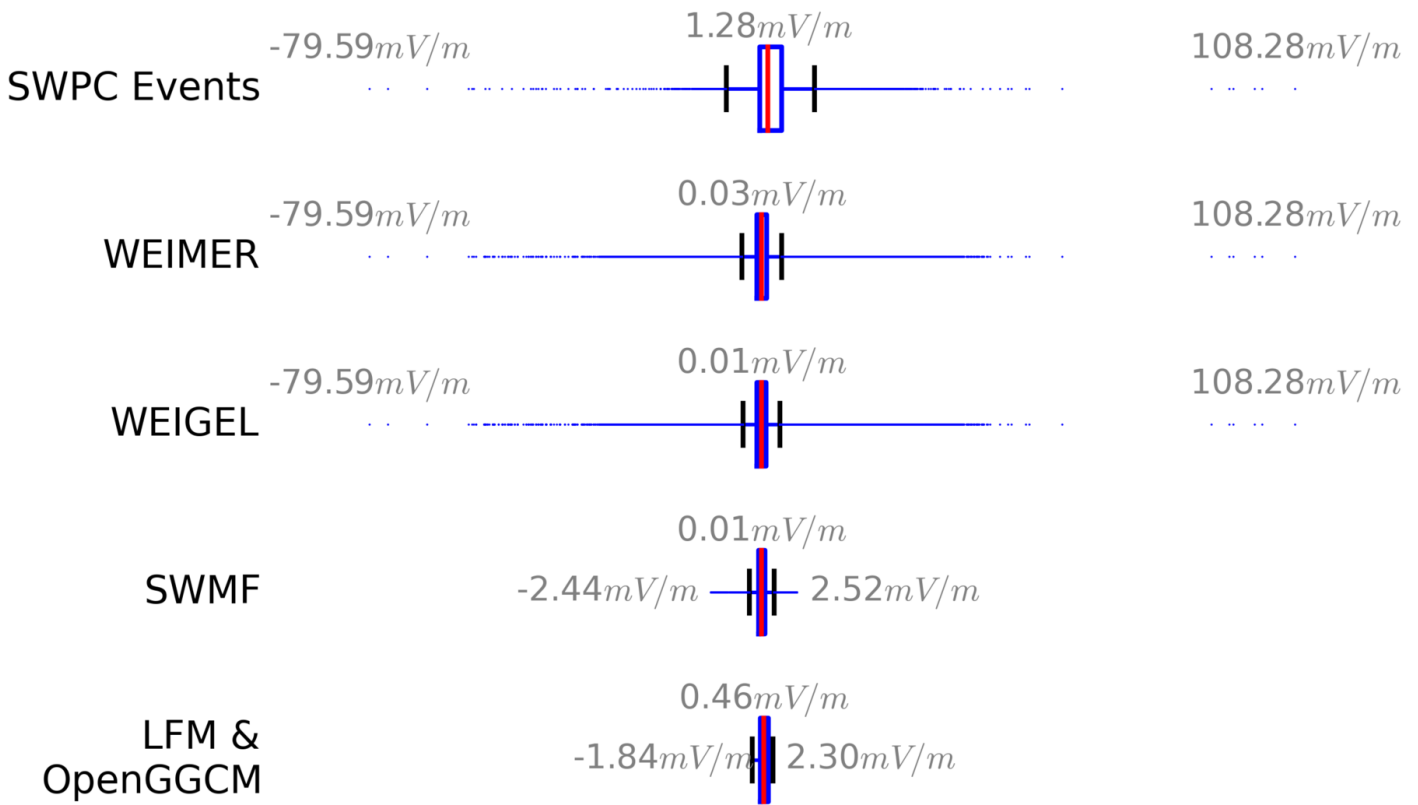
Figure 5. Comparison of median error values, both ΔB (top row) and dB/dt (bottom row), for all models, as a function of VB_Z (left hand frames) and Sym-H (right hand frames).

Figure 6. Comparison of median ΔB errors at high latitude stations (dashed lines), mid latitude stations (dotted lines) and all stations combined (solid lines) for all models (different colors/frames). Left hand column shows median error as a function of VB_Z , right hand column shows error as a function of Sym-H.

Figure 7. Same as Figure 6 but for dB/dt error.

ot

Input Conditions: VB_Z



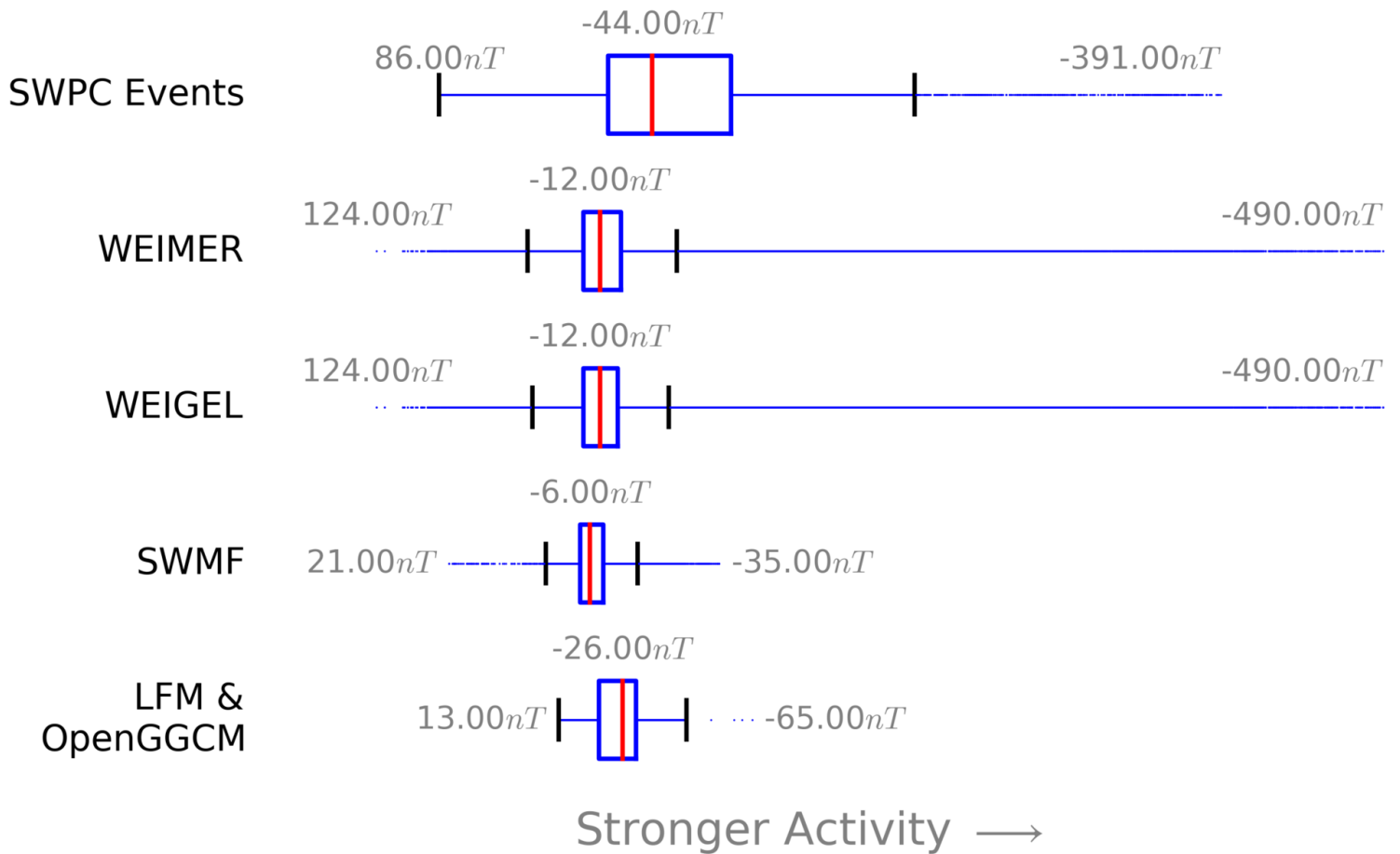
Stronger Driving →

2016SW001505-f01-z-.png

Al

ot

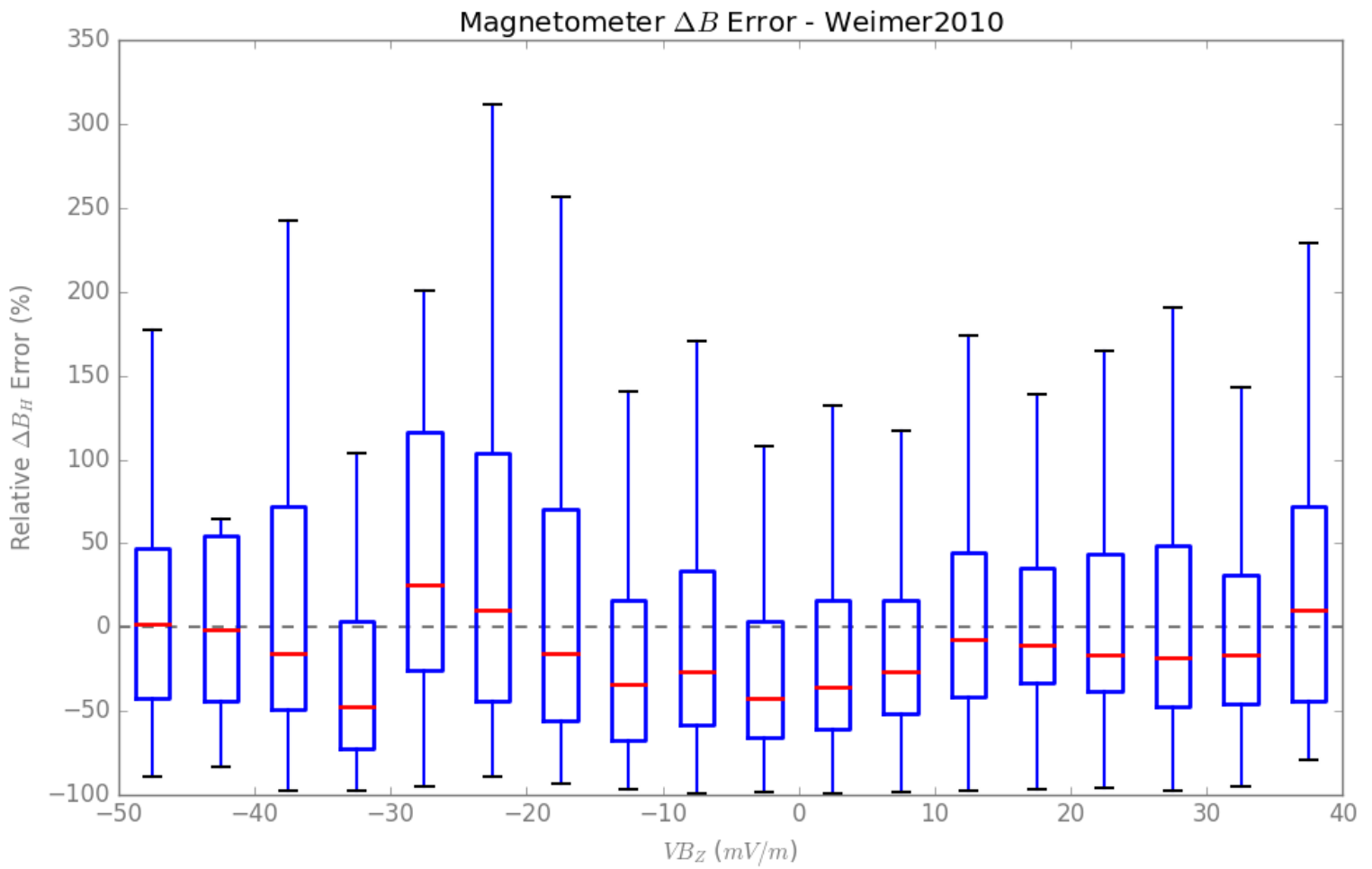
Input Conditions: Sym-H



2016SW001505-f02-z-.png

AI

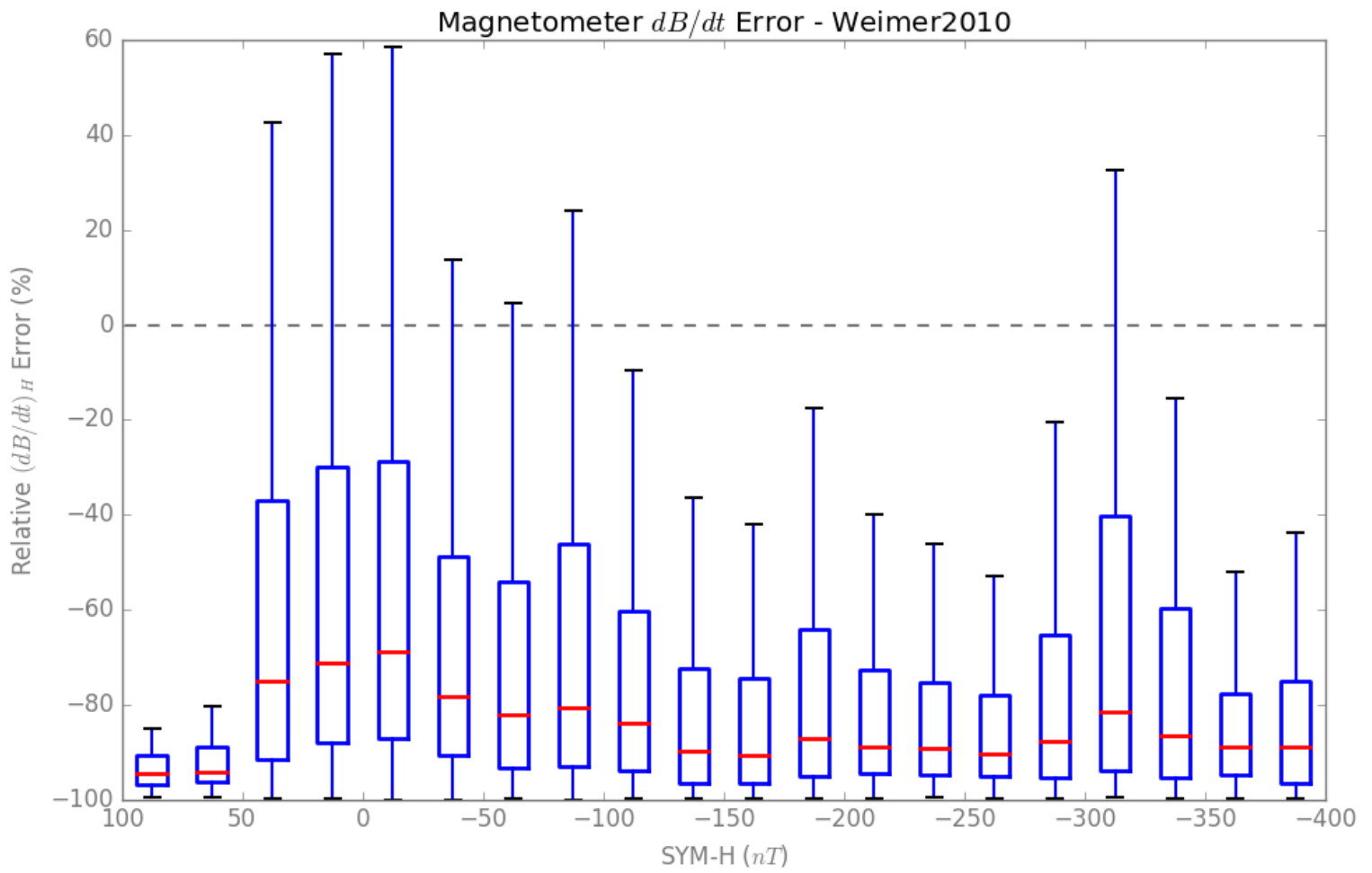
pt



2016SW001505-f03-z-.png

AL

pt



2016SW001505-f04-z-.png

AL

— LFM-MIX — SWMF — Weimer2010 — Weigel — OpenGGCM

